

Journal of Materials Chemistry C

Accepted Manuscript



This is an *Accepted Manuscript*, which has been through the Royal Society of Chemistry peer review process and has been accepted for publication.

Accepted Manuscripts are published online shortly after acceptance, before technical editing, formatting and proof reading. Using this free service, authors can make their results available to the community, in citable form, before we publish the edited article. We will replace this *Accepted Manuscript* with the edited and formatted *Advance Article* as soon as it is available.

You can find more information about *Accepted Manuscripts* in the [Information for Authors](#).

Please note that technical editing may introduce minor changes to the text and/or graphics, which may alter content. The journal's standard [Terms & Conditions](#) and the [Ethical guidelines](#) still apply. In no event shall the Royal Society of Chemistry be held responsible for any errors or omissions in this *Accepted Manuscript* or any consequences arising from the use of any information it contains.

Cite this: DOI: 10.1039/c0xx00000x

www.rsc.org/xxxxxx

ARTICLE TYPE

Radiative and non-radiative decay rate of $\text{K}_2\text{SiF}_6:\text{Mn}^{4+}$ phosphors

Minseuk Kim,^a Woon Bae Park,^a Bokeuk Bang,^b Chang Hae Kim,^b and Kee-Sun Sohn^{*a}

Received (in XXX, XXX) Xth XXXXXXXXX 20XX, Accepted Xth XXXXXXXXX 20XX

DOI: 10.1039/b000000x

⁵ Mn^{4+} -activated K_2SiF_6 phosphors for use in light emitting diode (LED) applications have recently attracted a great deal of attention since they exhibit an advantage over conventional wide band-type, red-light-emitting phosphors. $\text{K}_2\text{SiF}_6:\text{Mn}^{4+}$ phosphors have shown extremely narrow emission peaks in wavelengths that range from 620 to 630 nm, leading to a higher color-rendering index and larger color gamut for the final LED applications. We examined the decay behavior in terms of radiative and non-radiative rates along with a reliable evaluation of Mn^{4+} concentrations. Inter-activator energy transfer played a significant role in the luminescent process in this well-known narrow peak emission type of red phosphor, $\text{K}_2\text{SiF}_6:\text{Mn}^{4+}$.

Introduction

The need for a narrow-band red phosphor has been an important issue in view of the color-rendering index and color gamut for phosphor-converted LED. The Mn^{4+} -activated phosphor has attracted a great deal of attention in this regard and $\text{K}_2\text{SiF}_6:\text{Mn}^{4+}$ phosphors have recently been of particular interest. The ${}^2\text{E} \rightarrow {}^4\text{A}_2$ transition peaks with local vibronic modes of the MnF_6 octahedron in K_2SiF_6 produce narrow emission bands at around 625 nm, leading to a favorable red color in the field. Although most investigations have focused on the synthesis and photoluminescence of $\text{K}_2\text{SiF}_6:\text{Mn}^{4+}$ phosphors in association with a precise energy level assignment analysis [1-2], the decay behavior has rarely been examined. Although raw decay data have been reported several times, [3-5] an in-depth study on the decay behavior of $\text{K}_2\text{SiF}_6:\text{Mn}^{4+}$ has never been conducted in association with the energy transfer scheme.

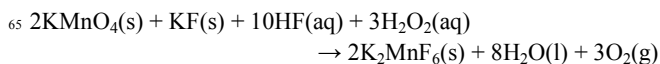
The decay behavior also deserves to be investigated from a practical point of view because a relatively long decay time in the msec. range for $\text{K}_2\text{SiF}_6:\text{Mn}^{4+}$ phosphors would cause problems when used in high-power LEDs. Moreover, if an ac-driven LED chip adopted such a long decay time, this also could be problematic. Consequently, the decay behavior of Mn^{4+} doped phosphors should be a reliable test of their applicability in LEDs. In the present investigation we examined the decay curves of $\text{K}_2\text{SiF}_6:\text{Mn}^{4+}$ in detail for both relatively low and high Mn^{4+} concentrations, and systematically evaluated the radiative and non-radiative decay rates. In particular, the non-radiative decay behavior affected by the inter-activator energy transfer was examined in association with a reliable estimation of the Mn^{4+} activator concentration based on inductively coupled plasma mass spectrometry (ICP-MS), energy-dispersive X-ray spectroscopy (EDS), and X-ray photoelectron spectroscopy (XPS) measurements.

We avoided inaccuracies in the measurement of critical energy

transfer distance (R_c) based on concentration quenching data, obtained by plotting luminescent intensity as a function of the activator concentration without a precise estimation of activator concentration. Instead, the R_c was evaluated using decay curves in association with an accurate estimation of Mn^{4+} activator concentration. More importantly, the radiative rate was evaluated using an extremely diluted form of $\text{K}_2\text{SiF}_6:\text{Mn}^{4+}$, the Mn^{4+} activator concentration of which was approximately below the measurement limit of both the ICP-MS and the XPS.

Experimental Procedures

The raw materials used for the synthesis were KMnO_4 (Junsei Chemical Co., Ltd. 99.3%), a solution of H_2SiF_6 (SAMCHUN 40 wt.%), a solution of HF (Avantor wt. 49%), H_2O_2 (SAMCHUN 34.5 wt.%), KF (High Purity Chemicals 99%). The synthesis of $\text{K}_2\text{SiF}_6:\text{Mn}^{4+}$ was achieved using a conventional precipitation method in the HF solution. First, we prepared K_2MnF_6 as a Mn^{4+} source based on the following reaction.



A stoichiometric amount of KF and K_2MnF_6 was dissolved in HF and mixed with a solution of H_2SiF_6 , then stirred for 15 min. When the precipitation was completed the solution was filtered and the filtrate was washed in acetone several times, and finally dried at 100 °C.

X-ray powder diffraction (XRD) method was used for the phase identification and EDS and ICP-MS were used for composition verification. XPS measurement was used to examine the valence state of the manganese ions, for obtaining a correct concentration of Mn^{4+} . The time-resolved photoluminescence (TRPL) spectra were measured using an in-house photoluminescence system involving a picosecond Nd:YAG (Continuum, Santa Clara, CA) laser with an excitation

wavelength of 355 nm and a charge-coupled device (CCD) sensor with a time resolution of 10 ns. We fixed both the delay time and the gate time at 0.2 ms for every measurement. The continuous wave photoluminescence (CWPL) spectra were also measured using an in-house spectroscope equipped with a xenon lamp at an

Experimental results and Discussion

Two $\text{K}_2\text{SiF}_6:\text{Mn}^{4+}$ phosphors were prepared with starting Mn^{4+} concentrations preset as 0.01 and 10 at.%, which hereafter are referred to as samples A and B, respectively. However, the Mn^{4+} concentration was not easily controlled during the precipitation process in the solution. Thus, the desired processing compositions, 0.01 and 10 at.%, were not realized in the final samples. The ICP-MS analyses identified the actual Mn concentration to be 'non-detectable' for sample A and 4~5 wt.% for sample B. The average Mn concentration obtained from the ICP measurement (4.695 wt.% or 2.46 at.%) will hereafter be referred to as the standard. Considering sensitivity limit of 0.001 wt.% for the ICP measurement of Mn ion, the actual Mn concentration should be lower than 0.001 wt.% for sample A.

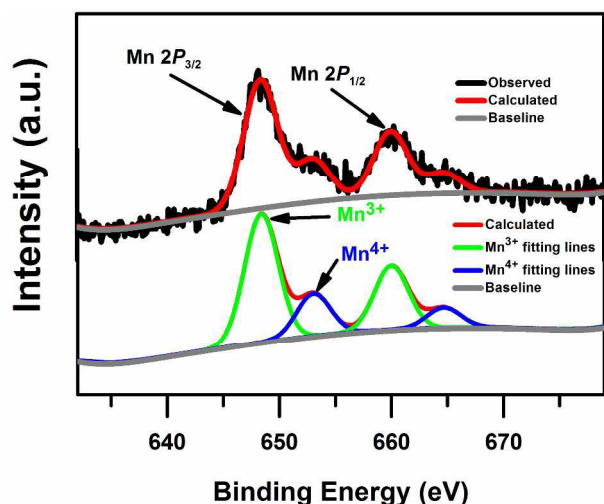


Fig. 1 Mn 2p core-level X-ray photoelectron spectra for $2p_{1/2}$ and $2p_{3/2}$ of Mn^{3+} and Mn^{4+} . The solid line designates the fitted lines.

It was more accurate to estimate the Mn^{4+} concentration out of the total concentration of Mn ions in various valence states, which was obtained from the ICP-MS measurement. XPS was used to accomplish this for sample B. Fig. 1 shows the Mn 2p core-level X-ray photoelectron spectrum together with fitted lines. The spectrum consists of $2p_{1/2}$ and $2p_{3/2}$ of Mn^{3+} and Mn^{4+} . The relative ratio between the different valence states (+3 and +4) of Mn ions for sample B was evaluated from the XPS data using a simple regression-fitting process, as shown in Fig. 1. It was obvious that Mn^{3+} ions were present along with Mn^{4+} ions in sample B. A rough estimate of the relative portion of Mn^{4+} was established to be 24% from the simple regression fitting of XPS spectra for both $2p_{1/2}$ and $2p_{3/2}$ peaks. The ICP-MS measurement of Mn content (2.46 at.%) was reduced to 0.59 at.% when considering only the activator (Mn^{4+}) concentration. This meant that only about 5% of the starting Mn content (10 at.%) was incorporated as Mn^{4+} activators in the K_2SiF_6 host, and the other

95% might have been dissolved in the solution and wasted during the synthesis or existed as Mn^{3+} in the K_2SiF_6 host. As the XPS results showed, a considerable number of Mn^{3+} resided in the K_2SiF_6 host, which was, in fact, much higher than the number of Mn^{4+} activators. Mn^{3+} has $3d^4$ configurations consisting of one spin-quintet (^5D), five spin-triplets (^3D , $^3\text{F}_{1,2}$, ^3G , ^3H), and eight spin-singlets ($^1\text{S}_{1,2}$, $^1\text{D}_{1,2}$, ^1F , $^1\text{G}_{1,2}$, ^1I) [7]. The crystal field splitting of these term symbols constitutes a much more complicated energy level, but there was no energy transition leading to visible light emission in any of the host materials at room temperature.

It was impossible to measure the Mn concentration for sample A from the EDS and ICP-MS measurements due to the lower activator concentration. Moreover, the Mn^{4+} activator concentration for sample A should have been much lower than what could be inferred from the measurement limits of EDS and ICP. This implied that we had reached an extremely low Mn^{4+} activator concentration for this sample, and even this extremely low Mn^{4+} activator concentration was sufficient to measure the emission spectrum and in turn the radiative decay time for the $^2\text{E} \rightarrow ^4\text{A}_2$ emission of Mn^{4+} in the K_2SiF_6 host. Although the presence of Mn ions was not detectable in the EDS, XPS, or ICP-MS measurements, both CWPL and TRPL revealed an $^2\text{E} \rightarrow ^4\text{A}_2$ emission of Mn^{4+} in sample A, as shown in Fig. 2. Therefore, the measured decay time for this extremely low Mn^{4+} concentration of sample A could be regarded as a radiative decay time for the $^2\text{E} \rightarrow ^4\text{A}_2$ emission of Mn^{4+} in the K_2SiF_6 host. Because the multiphonon relaxation could be ignored for the emission in a visible range, the decay time measured for sample A could be the pure radiative decay time.

At least two phosphor samples, one with an extremely low Mn^{4+} concentration and the other with a relatively high Mn^{4+} concentration, were required to evaluate the radiative and non-radiative decay rates, which led to a systematic understanding of the inter-activator energy transfer behavior. In particular, the decay behavior of the Mn^{4+} activator in an extremely dilute system would be very important in understanding a radiative decay process with no influences from the inter-activator energy transfer. Although we were not able to measure the exact Mn^{4+} content for sample A by employing the above-described composition analysis tools, the emission spectrum was clearly detected in this diluted sample, as shown in Fig. 2. Therefore, it is certain that Mn^{4+} ions were present in this sample and the concentration was definitely below 0.001 wt%, which is the detection limit of the ICP-MS.

The emission and excitation spectra measured at continuous wave (CW) excitations are shown in Fig. 2 (a) for typical $^2\text{E} \rightarrow ^4\text{A}_2$ emission peaks with local vibronic modes of the MnF_6 octahedron in K_2SiF_6 and two broad excitation bands representing $^0\text{A}_2 \rightarrow ^4\text{T}_2$ (~460 nm) and $^0\text{A}_2 \rightarrow ^4\text{T}_1$ (~360 nm) transitions in the excitation spectrum. Because all the CW measurements were implemented at room temperature with a low-wavelength resolution, several vibronic side bands that include zero phonon lines were not detected. On the contrary, the TRPL spectra shown in Fig. 2 (b) and (c) clearly exhibited Stokes and anti-Stokes peaks for ν_3 , ν_4 , and ν_6 for both samples A and B.

Fig. 3 shows the XRD patterns of synthesized $\text{K}_2\text{SiF}_6:\text{Mn}^{4+}$, wherein it was confirmed that there were no impurity phases,

while the indexed peak location and its relative intensity followed the standard data of an Fm-3m symmetry with lattice parameters ($a = 8.134 \text{ \AA}$, $b = 8.134 \text{ \AA}$, $c = 8.134 \text{ \AA}$, $\alpha = 90^\circ$, $\beta = 90^\circ$, $\gamma = 90^\circ$). The morphologies of the synthesized KSF samples are shown as insets, and proved to be of typical polyhedron shapes with no texture. [6]

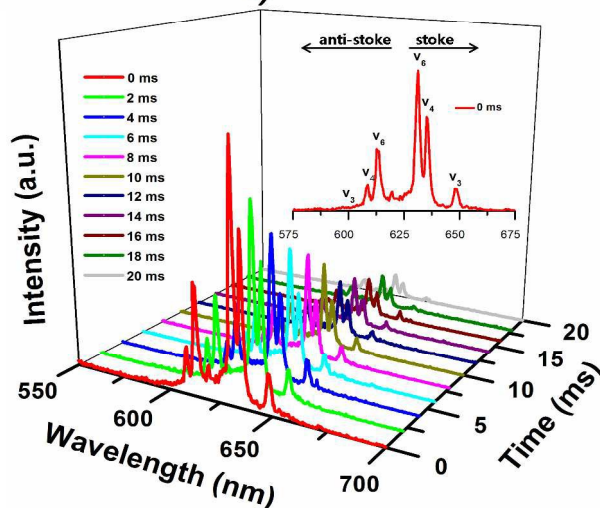
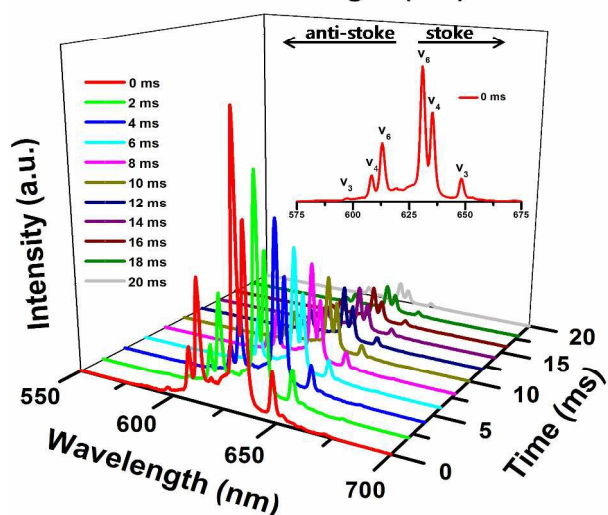
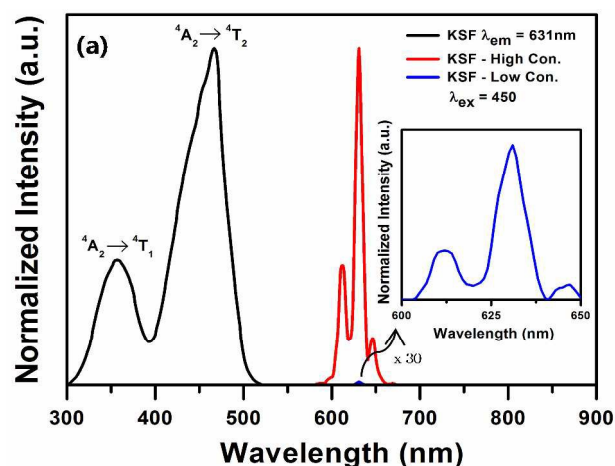


Fig. 2 (a) The excitation and emission spectra of $\text{K}_2\text{SiF}_6:\text{Mn}^{4+}$ under CW conditions, (b) and (c) the time-resolved emission spectra for a $\text{K}_2\text{SiF}_6:\text{Mn}^{4+}$ phosphor measured via Nd:YAG laser as an exciting light source for samples A and B.

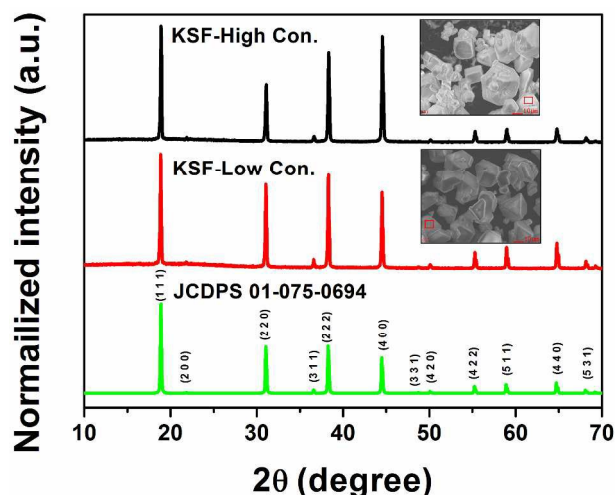


Fig. 3 High- and low-concentration XRD patterns of $\text{K}_2\text{SiF}_6:\text{Mn}^{4+}$ compared with the standard JCDPS 01-075-0694.

Fig. 4 exhibits the decay curves for samples A and B, with the probe wavelength set at the location of the highest emission peak (v_6 vibronic side band). The decay curves detected at every vibronic side band wavelength all coincided, but in the interest of brevity the data are not given here. Fig. 4 shows the typical concentration quenching behavior, which is marked by the facilitated decay of the increased activator concentration. The $1/e$ decay time (τ) for sample A was 8.52 ms., which is believed to be indicative of the radiative decay time and the temperature-dependent phonon term for the ${}^2\text{E} \rightarrow {}^4\text{A}_2$ emission of Mn^{4+} in the K_2SiF_6 host. Namely, $1/\tau_{\text{A measured}} = 1/\tau_{\text{radiative}} + 1/\tau_{\text{phonon}}$.

The decay time was 7.43 ms. for sample B. The measured decay rate for sample B, which is the reciprocal of the measured decay time, was the sum of the radiative rate and the non-radiative rate terms (phonon and energy transfer), as shown by the following relationship:

$$\frac{1}{\tau_{\text{B measured}}} = \frac{1}{\tau_{\text{radiative}}} + \frac{1}{\tau_{\text{phonon}}} + \frac{1}{\tau_{\text{ET}}} \quad (1)$$

The radiative decay time was assumed to be 13 ms., which was measured by Kasa and Adachi [8] for a sufficiently diluted $\text{K}_2\text{SiF}_6:\text{Mn}^{4+}$ ($\text{Mn} < 1 \text{ at.}\%$) at low temperatures from 20 K up to about 100 K. The second term on the right-hand side comes from the effects of phonons (or temperature). The last term stands for the non-radiative energy transfer. Accordingly, the measured decay rate for sample B is the sum of the radiative rate (= measured decay rate for sample A) and the non-radiative rate ($1/\tau_{\text{non-radiative}} = 1/\tau_{\text{phonon}} + 1/\tau_{\text{ET}}$). According to Eqn. (1), the phonon-dependent term was calculated to be 40.45 s^{-1} , and the non-radiative energy transfer rate was calculated to be 17.22 s^{-1} for sample B. The average inter-activator distance (R) was calculated to be 35.2 \AA from the accurate Mn^{4+} concentration for sample B. Based on the definition of critical energy transfer distance (R_c), R_c was evaluated to be about 27.4 \AA through Eqn. (2), wherein a dipole-dipole interaction was assumed to dominate. By definition, R_c is the distance at which the radiative decay rate is equal to the non-radiative decay rate due to the non-radiative energy transfer.

$$\frac{1}{\tau_{B \text{ measured}}} = \frac{1}{\tau_{\text{radiative}}} \left(1 + \left(\frac{R_c}{R} \right)^6 \right) + \frac{1}{\tau_{\text{phonon}}}$$

$$\frac{1}{\tau_{ET}} = \left(\frac{R_c}{R} \right)^6 \frac{1}{\tau_{\text{radiative}}}$$
(2)

The evaluated R_c was slightly longer than the typical critical energy transfer distance for other types of activators, such as Eu^{3+} , Tb^{3+} , Eu^{2+} , Ce^{3+} , and Mn^{2+} , in various host structures [9-12]. Unfortunately we could find no reported value for the critical energy transfer distance (R_c) for Mn^{4+} in the K_2SiF_6 host. However, the critical energy transfer distances for Mn^{4+} in some other hosts were reported to be 8.6, 25.9, and 43.4 Å for $\text{La}_2\text{LiTaO}_6:\text{Mn}^{4+}$ [13], $\text{Sr}_4\text{Al}_{14}\text{O}_{25}:\text{Mn}^{4+}$ [14], and $\text{CaMg}_2\text{Al}_6\text{O}_{27}:\text{Mn}^{4+}$ [15], respectively. These R_c values were estimated in the conventional manner, that is, they were all obtained from the concentration quenching data. In particular, those R_c values were from the critical concentration (x_c), which is indicative of the highest PL intensity in the plot of PL intensity vs. activator concentration. It should be noted that the scattering R_c values might be ascribed to an incorrect Mn^{4+} concentration estimation, even though the different host materials would partially affect R_c .

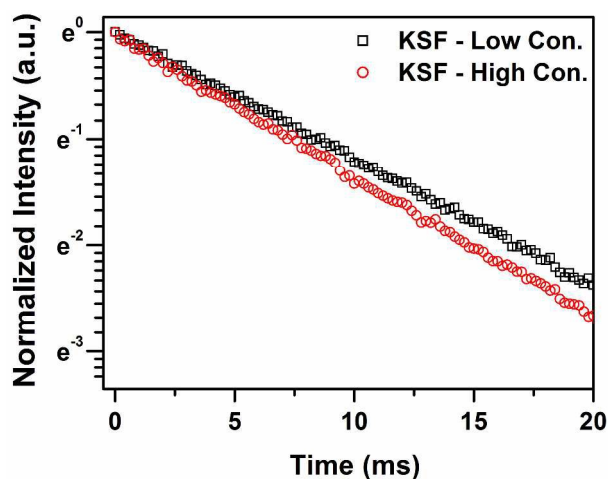


Fig. 1 Decay curves of $\text{K}_2\text{SiF}_6:\text{Mn}^{4+}$ for low (sample A) and high (sample B) Mn^{4+} concentrations ($\lambda_{\text{ex}} = 355\text{nm}$).

The true Mn^{4+} concentration was crucial in evaluating legitimate R_c values. It would be inappropriate to collect so-called concentration quenching data without a precise measurement of the concentration of Mn^{4+} activators. The R_c evaluation from the concentration quenching data based on the starting composition would not be appropriate without a post-analysis of the composition, because the Mn activator control in the synthesis process is complicated. We elicited an R_c value from the decay curve rather than from the concentration quenching data. Thereafter, the critical Mn^{4+} activator concentration was obtained in reverse from the R_c value that we obtained from the decay curve measurement, i.e., the measurement of both the reliable radiative decay time for sample A and the correct activator concentration for sample B. The following formula is a typical x_c vs. R_c relationship.

$$x_c = \left(\frac{6V}{\pi N R_c^3} \right)$$
(3)

where V is the unit cell volume of the K_2SiF_6 host and N is the number of Si sites in the K_2SiF_6 unit cell. The x_c was evaluated to be 1.55 at.%, which was greater than that of sample B (0.59 at.%). This never allowed us to incorporate 2.63 times more Mn^{4+} activator in the K_2SiF_6 host without a serious luminescence quenching in comparison with the Mn^{4+} activator concentration of sample B. The x_c in the present investigation was not an activator concentration corresponding to the maximum PL intensity, which nonetheless is regarded as a conventional x_c in most phosphor-related reports. It was taken for granted that x_c could be elicited from the so-called concentration quenching data, so that PL intensity data was monitored as a function of the activator concentration, and thereafter the x_c value was used for the evaluation of R_c . However, the x_c in the present investigation was obtained from the R_c , and the R_c value was determined from the decay curve by more strictly obeying the definition of R_c , which is a distance at which the non-radiative energy transfer rate is equal to the radiative rate. In other words, the maximum PL intensity does not necessarily have to coincide with x_c in the present case.

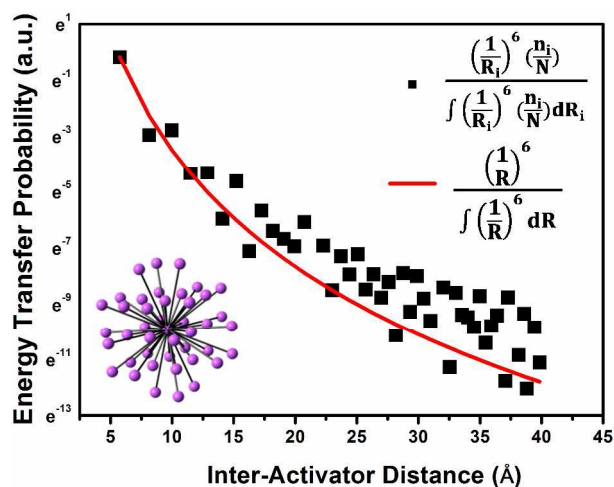


Fig. 2 The energy transfer probability density function as a function of the inter-activator distance for Mn^{4+} distribution in homogeneous (solid line) and crystal (dots) hosts. The inset shows the short-range local structure of the Si site distribution in the K_2SiF_6 host (up to 10 Å).

The non-radiative process takes place mainly through inter-activator energy transfer and through the ensuing quenching in the killer site in most phosphors. Therefore, the inter-activator distance and the activator distribution in the host play significant roles in the energy transfer process. Vázquez has argued that the decay rate strongly depends on the geometrical factor indicating the energy transfer route in a specific crystal structure [16-19]. The non-homogeneous activator distribution in the crystalline host as shown in Fig. 5 was taken into account systematically in his reliable mathematical model. In addition, we have reconfirmed the model in several LED phosphors [20-22]. Since the K_2SiF_6 host has a well-crystallized structure, the activator distribution is not homogeneous, but is restricted by the Si site distribution in the K_2SiF_6 structure. Because the Mn^{4+} activator occupies only the Si site, it is obvious that the inter-activator energy transfer takes place among the Si site in the K_2SiF_6 crystalline host. The energy transfer probability density function

was plotted with respect to an inter-activator distance of as much as 40 Å, as shown in Fig. 5, which allowed a systematic comparison between the homogeneous distribution and the crystal site-involved distribution. The former was $\sim(1/R)^6$ and the latter was $(1/R_i)^6(n_i/N)$, and both were normalized by the area under the curves, wherein R is an averaged distance while R_i represents the distance to the i^{th} neighbors, n_i is the number of neighbors, and N is the total number of Si sites within the radius of 40 Å. There was a slight difference between homogeneous and crystal distributions. The energy transfer probability (or rate) in the crystalline host should be slightly higher than the homogeneous distribution case, particularly for a larger distance, as shown in Fig. 5.

Conclusions

The decay curves were analyzed for two $\text{K}_2\text{SiF}_6:\text{Mn}^{4+}$ phosphors. The first had an extremely low Mn concentration, which simulated an ideal, dilute system for a radiative decay rate measurement, and the second had a conventional Mn concentration for an acceptable PL efficiency for use in LED applications. Rather than the typical approach to obtain R_c from the conventional concentration quenching data, we obtained the R_c value from the decay curve measurement based on the definition of R_c . Namely, it was possible to compute R_c based on the definition of R_c , along with the radiative decay rate obtained from the extremely low Mn concentration and the precise measurement of Mn^{4+} activator concentration. Since it was difficult to predict the real Mn^{4+} activator concentration from the starting composition, a reliable post analysis of the final sample composition was required based on EDS, XPS, and ICP. The decay measurement for both the $\text{K}_2\text{SiF}_6:\text{Mn}^{4+}$ model phosphors was useful for an accurate estimation of R_c , and, in turn, led to a better understanding of the energy transfer behavior of $\text{K}_2\text{SiF}_6:\text{Mn}^{4+}$. The activator site distribution had a great deal of influence on the non-radiative energy transfer and in turn on the decay behavior of $\text{K}_2\text{SiF}_6:\text{Mn}^{4+}$.

Acknowledgement

This work was supported by the National Research Foundation of Korea Grant funded by the Korean Government (NRF-2013R1A2A2A04015089) and partly supported by partly by the Technology Innovation Program (or Industrial Strategic technology development program, 10050315, Discovery of narrow emission red phosphors for use in large color gamut and high power LEDs) funded By the Ministry of Trade, industry & Energy (MI, Korea).

Notes and references

^a Faculty of Nanotechnology and Advanced Materials Engineering, Sejong University, Seoul 143-747, Korea. Fax: 82 2 3408 4477; Tel: 82 2 3408 4477; E-mail: kssohn@sejong.ac.kr

^b Korea Research Institute of Chemical Technology, Daejeon 305-600, Korea. Fax: 82 42860 7508; Tel: 82 42 860 7374;

- 1 J. H. Oh, H. Kang, H. K. Park and Y. R. Do, *J. Mater. Chem. C*, 2015, **3**, 607-615.
- 2 T. Takahashi and S. Adachi, *J. electrochem. Soc.*, 2008, **155**, E183-E188.

- 3 H. -D. Nguyen, C. C. Lin, M. -H. Fang and R.-S. Liu, *J. Mater. Chem. C*, 2014, **2**, 10268-10272.
- 4 T. Oyama and S. Adachi, *J. Appl. Phys.*, 2014, **116**, 133515.
- 5 T. Nakamura, Z. Yuan and S. Adachi, *Appl. Surf. Sci.*, 2014, **320**, 514-518.
- 6 J. H. Loehlin, *Acta Crystallogr.*, 1984, **C40**, 570.
- 7 N. M. Avram and M. G. Brik, *Optical Properties of 3d-Ions in Crystals: Spectroscopy and Crystal Field Analysis*, Tsinghua University Press, Beijing, and Springer-Verlag, Berlin Heidelberg, 2013, Ch. 2, pp. 70-73.
- 8 R. Kasa and S. Adachi, *J. Electrochem. Soc.*, 2012, **159**, J89-J95.
- 9 K. -S. Sohn, E. S. Park, C. H. Kim and H. D. Park, *J. Electrochem. Soc.*, 2000, **147**, 4368-4373.
- 10 S. Y. Seo, K. -S. Sohn, H. D. Park and S. Lee, *J. Electrochem. Soc.*, 2002, **149**, H12-H18.
- 11 Y. Jin and Y. Hu, *J. Alloys Compd.*, 2014, **610**, 695-700.
- 12 J. Zhang, L. Wang, Y. Jin, X. Zhang, Z. Hao and X. -J. Wang, *J. Lumin.*, 2011, **131**, 429-432.
- 13 L. Wang, L. Yuan, Y. Xu, R. Zhou, B. Qu, N. Ding, M. Shi, B. Zhang, Y. Chen, Y. Jiang, D. Wang and J. Shi, *Appl. Phys. A*, 2014, **117**, 1777-1783.
- 14 M. Peng, X. Yin, P. A. Tanner, C. Liang, P. Li, Q. Zhang and J. Qiu, *J. Am. Ceram. Soc.*, 2013, **96**, 2870-2876.
- 15 B. Wang, H. Lin, J. Xu, H. Chen and Y. Wang, *ACS Appl. Mater. Interfaces*, 2014, **6**, 22905-22913.
- 16 S. O. Vásquez, *J. Chem. Phys.*, 1996, **104**, 7652-7657.
- 17 S. O. Vásquez, *J. Chem. Phys.*, 1997, **106**, 8664-8671.
- 18 S. O. Vásquez, *Phys. Rev. B*, 1999, **60**, 8575-8585.
- 19 S. O. Vásquez, *Phys. Rev. B*, 2001, **64**, 125103-1-7.
- 20 W. B. Park, T. H. Kwon and K. -S. Sohn, *J. Am. Ceram. Soc.*, 2015, **98**, 490-494.
- 21 Y. W. Jung, B. Lee, S. P. Singh and K. -S. Sohn, *Opt. Express*, 2010, **18**, 17805-17818.
- 22 W. B. Park, Y. Song, M. Pyo and K. -S. Sohn, *Opt. Lett.*, 2013, **38**, 1739-1741.